Geotech Geol Eng (2026) 44:407
https://doi.org/10.1007/s10706-026-03867-3

ORIGINAL PAPER

The Tricky Water Energy Budget of Freezing Soil: A Thermodynamic Framework for Understanding Phase Changes

John Mohd Wani · Concetta D'Amato · Riccardo Rigon

Received: 31 December 2025 / Accepted: 19 August 2026
© The Author(s) 2026

Abstract Freezing soil presents unique challenges in understanding the coupled mass and energy dynamics within the Earth's critical zone. This paper focuses on the thermodynamic energy budget of pore water within a rigid soil skeleton, and presents a thermodynamic framework for analysing phase transitions in soil–water-ice systems. Three elements, so far treated separately in the hydrological, geotechnical and physical-chemistry literatures, are assembled here into a single self-consistent chain: (i) a unified derivation of freezing point depression integrating capillary (Gibbs-Thomson), osmotic, and adsorptive mechanisms through a single chemical-potential decomposition; (ii) an explicit thermodynamic derivation of the Soil Freezing Characteristic Curve (SFCC) from the Soil Water Retention Curve (SWRC) via the generalised Clausius-Clapeyron relation, incorporating Lu's adsorption-aware retention model; and (iii) the connection of the SFCC to a Darcy-scale enthalpy balance as a constitutive closure. Temperature, pressure and chemical potential act as the driving forces, but every constitutive relation derived here assumes local thermodynamic equilibrium within each representative elementary volume, i.e., the framework is non-equilibrium at the Darcy scale and equilibrium at the pore scale. Rate-dependent behaviour is identified as an open problem, not resolved. The framework accounts for freezing point depression through mechanisms including the Gibbs-Thomson effect, solute presence, ice nucleation, and surface interactions. We demonstrate how upscaling from pore-scale thermodynamics to the Darcy scale introduces theoretical challenges in determining phase transformation rates and flux laws. The sequential freezing process, governed by water energetic states in different pore sizes, creates complex interplay between capillary forces and phase changes essential for modeling permafrost dynamics and seasonal freeze-thaw cycles. The contribution is theoretical as no new measurements are reported, and quantitative validation against measured soil freezing characteristic curves is deferred to a companion paper. The framework rests on three assumptions:

John Mohd Wani and Concetta D'Amato contributed equally to this work.

J. M. Wani · C. D'Amato · R. Rigon
C3A - Center Agriculture Food Environment, University of Trento, Via Edmund Mach, 1 San Michele all'Adige, 38098 Trento, Italy
e-mail: johnmohd.wani@unitn.it

C. D'Amato
e-mail: concetta.damato@epfl.ch

C. D'Amato · R. Rigon (✉)
Department of Civil, Environmental and Mechanical Engineering, University of Trento, Via Mesiano 77, 38123 Trento, Italy
e-mail: riccardo.rigon@unitn.it

C. D'Amato
Laboratory of Catchment Hydrology and Geomorphology, EPFL Valais Wallis, Route des Ronquos 86, 1951 Sion, Valais, Switzerland

Published online: 08 October 2026

local equilibrium, instantaneous redistribution of water within a representative elementary volume, and the "freezing = drying" analogy. Each is therefore stated explicitly, together with the conditions under which it is expected to fail.

Keywords Freezing soil · Permafrost · Local thermodynamic equilibrium · Freezing point depression · Soil freezing characteristic curve

List of Symbols

T	Temperature K
T_0	Bulk freezing point of water (273.15 K) K
T^*	Pore-scale freezing point K
T_{ref}	Reference temperature in enthalpy definition (= T_0 here) K
p	Pressure Pa
μ_w, μ_{ice}	Chemical potential of water / ice J mol^{-1}
a_w	Water activity (dimensionless) –
R	Universal gas constant (8.314 J mol^{-1} K^{-1}) J mol^{-1} K^{-1}
H	Enthalpy per unit volume J m^{-3}
C_p	Bulk volumetric heat capacity J m^{-3} K^{-1}
$c_{p,\alpha}$	Specific heat capacity of phase α J kg^{-1} K^{-1}
$\mathcal{L}_f$	Molar latent heat of fusion (≈6012 J mol^{-1}) J mol^{-1}
ℓ_f	Specific latent heat of fusion (≈334 000 J kg^{-1}) J kg^{-1}
M_w	Molar mass of water (0.018 kg mol^{-1}) kg mol^{-1}
ρ_α	Density of phase α kg m^{-3}
θ_α	Volumetric fraction of phase α m^3 m^{-3}
θ^{tot}	Total water content ($\theta_w + \theta_i$) m^3 m^{-3}
$\mathbf{J}_H$	Total energy flux W m^{-2}
$\mathbf{J}_T$	Conductive heat flux W m^{-2}
$\mathbf{J}_w$	Water flux (Darcy) m s^{-1}
λ_{eff}	Effective thermal conductivity W m^{-1} K^{-1}
K	Hydraulic conductivity m s^{-1}
ψ_p	Matric potential expressed as a pressure (< 0) Pa
ψ	Matric (pressure) head ($= \psi_p/\rho_w g, < 0$) m
s	Suction ($= -\psi_p, > 0$) Pa
$s_{\max}, s_c$	Oven-dry suction; mean cavitation suction Pa
$(\psi + z)$	Hydraulic head m
z	Elevation head m
$\bar{v}_w$	Molar volume of water m^3 mol^{-1}
g	Gravitational acceleration m s^{-2}
r	Pore radius m (or μm where stated)
$r^*(T)$	Critical pore radius at temperature T m
$f(r)$	Pore-size probability density function m^{-1}
σ	Surface tension of water J m^{-2}
γ_{iw}	Ice-water interfacial tension (≈0.029 J m^{-2}) J m^{-2}
K_{GT}	Gibbs–Thomson coefficient (≈0.052 K μm) K m
α	Contact angle rad
α_{vG}, n	Retention parameters, Eq. 26 Pa^{-1}, –
i	Van 't Hoff factor (ion count per formula unit) –
c	Molar concentration of solute mol m^{-3}
π	Osmotic pressure Pa
ΔT	Freezing point depression ($T^* - T_0$) K
θ_a, θ_c	Adsorbed / capillary water content m^3 m^{-3}
θ_{sat}	Saturated water content (Eq. 26) m^3 m^{-3}
$\tau_{intra}, \tau_{inter}$	Intra-/inter-REV timescales s
Da_c	Timescale ratio $\tau_{intra}/\tau_{inter}$
$\bar{v}_i$	Molar volume of ice ($= M_w/\rho_i$) m^3 mol^{-1}

1 Introduction

The physics of freezing soil represents one of the most complex problems in environmental science, combining elements of non-equilibrium thermodynamics (Groot and Mazur 1984), fluid mechanics in porous media (Muskat and Meres 1936), and phase transition theory (Lunardini 1985). Unlike pure water systems, soil–water-ice interactions involve multiple phases coexisting under varying thermodynamic conditions, with phase boundaries depending not only on temperature but also on pressure, chemical composition, and interfacial effects (Watanabe and Flury 2008; Zhang et al. 2022). The phenomenon of permafrost is closely linked to freezing soil dynamics, and is defined thermally as the ground material that remains below 0°C for at least two consecutive years (Lewkowicz et al. 2025). Most importantly, the presence of ice is not necessary, and the term refers to any ground material (Dobinski 2012).

Permafrost underlies approximately 24% of the Northern Hemisphere's exposed land surface (Zhang

et al. 1999; Obu et al. 2019) and stores vast quantities of organic carbon. Its thermal stability has profound implications for infrastructure (Hjort et al. 2018), carbon cycle (Schuur and McGuire 2015), and hydrological processes (Walvoord and Kurylyk 2016) under changing climate (Schuur and McGuire 2015). Infrastructure in cold regions, from pipelines to buildings to transportation networks, depends critically on accurate prediction of freeze-thaw dynamics. The theoretical analysis of freezing soil physics involves several interconnected aspects: the energetic state of partially frozen soil and its relationship to water and ice contents through the generalised Clausius-Clapeyron relations (Dall'Amico et al. 2011); the hydraulic conductivity of water under frozen conditions, which requires extensions of classical unsaturated flow theory (Watanabe and Osada 2016; Kurylyk and Watanabe 2013); and the depression of freezing temperature relative to bulk water, governed by capillary effects (Gibbs-Thomson) (Wettlaufer and Worster 2006), solute concentration (Amankwah et al. 2021), nucleation barriers (Wang et al. 2023), and surface adsorption forces (Devoie et al. 2022; Zhang et al. 2022b). Finally, these governing thermodynamic laws must be upscaled to the Darcy scale. Rigorous mathematical upscaling from pore-scale Stefan problems to Darcy-scale effective models has been established by Peszynska et al. (2024a, 2024b); permafrost field modelling relies on empirical unfrozen-water parameterisations of the type reviewed in Romanovsky and Osterkamp (2000); and engineering models of cryosuction and frost heave have been developed by Michalowski and Zhu (2006); Rempel et al. (2004), though many remain semi-empirical (Stuurop et al. 2021).

The general aim of this paper is to develop a thermodynamic framework for analysing phase transitions in soil–water-ice systems. By using the "freezing equals drying" (Koopmans and Miller 1966) hypothesis, we aim to bridge the gap between pore-scale physics and macroscopic flow laws. This study integrates the Gibbs-Thomson effect with surface forces to provide a strong theoretical basis for predicting mass and energy transport in permafrost environments.

The paper has four specific objectives: (1) To derive the freezing point depression of pore water from a single decomposition of the water chemical potential, so that the capillary (Gibbs–Thomson), osmotic (Raoult / van 't Hoff) and adsorptive contributions appear as terms of one expression rather than as three separate models. (2) To obtain the Soil Freezing Characteristic Curve (SFCC) from the Soil Water Retention Curve (SWRC) through the generalised Clausius–Clapeyron relation, using a retention model that resolves adsorbed as well as capillary water. (3) To close the Darcy-scale enthalpy balance with the resulting SFCC, so that temperature, liquid water content and ice content follow from a single conserved state variable. (4) To state, and examine critically, the assumptions on which (1)–(3) rest: local thermodynamic equilibrium, instantaneous redistribution of water within a representative elementary volume (REV), and the "freezing = drying" analogy. For each we identify the conditions under which it is expected to fail.

The enthalpy form of the energy budget (Dall'amico 2010; Tubini et al. 2021), the Darcy–Buckingham flux law (Buckingham 1907; Richards 1931b), the Young–Laplace and Gibbs–Thomson relations (Young 1805; Wettlaufer and Worster 2006), Raoult's law and the van 't Hoff relation (Raoult 1886; Hoff 1887), Lu's adsorption-aware retention model (Lu 2016) and the generalised Clausius–Clapeyron mapping between suction and freezing temperature (Dall'Amico et al. 2011) are all established results, reproduced below only to keep the chain of reasoning self-contained and to fix one notation across literatures that use different conventions.

This paper assembles them into a single, internally consistent chain and makes explicit what that assembly assumes: (i) a unified derivation of freezing point depression that integrates capillary (Gibbs-Thomson), osmotic (van 't Hoff/Raoult), and adsorptive contributions through a single chemical-potential decomposition, with the conditions for the additivity of the three contributions made explicit (Eq. 13); (ii) an explicit thermodynamic derivation of the SFCC from the SWRC using the generalised Clausius-Clapeyron relation, incorporating the adsorption-aware retention framework of Lu (2016), together with a statement of the five assumptions that this isomorphism requires; (iii) the connection of the SFCC to the Darcy-scale enthalpy balance as a constitutive closure, consistent with the WHETGEO implementation of Tubini and Rigon (2022); and (iv) a timescale criterion (Eq. 9) that turns the local-equilibrium and instantaneous-redistribution hypotheses from unstated assumptions into a condition that can be tested. The paper

is therefore a synthesis whose assumptions can be tested, not a new constitutive law: no new flux law, no new retention model and no new measurements are presented. The paper is explicitly limited to the energy budget of pore water within a rigid, non-deformable soil skeleton. Frost-heave mechanics and ice-lens formation (Rempel et al. 2004; Dash et al. 2006) lie outside this scope. Experimental validation is deferred to a companion paper that will couple the framework to the Richards equation and compare against measured SFCC data.

Section 2 introduces the enthalpy-based energy budget and the Darcy-scale conservation equations. Section 3 presents the Darcy-Buckingham flux law and discusses the local-equilibrium upscaling assumptions. Section 4 derives the freezing point depression from capillary, osmotic, and adsorptive contributions and shows how the SFCC is obtained from the SWRC. Section 5 summarises conclusions and future directions.

2 Thermodynamic Framework

This section develops the energy budget for the pore-water subsystem (liquid water, ice, and air) within a rigid, non-deformable soil skeleton. The solid matrix enters only as a passive thermal mass through the bulk heat capacity C_p. Mechanical deformation, frost heave, and ice-lens formation are not considered, nor is the work done against the skeleton by the volume change that accompanies freezing.

In non-equilibrium thermodynamics, system evolution is governed by three main thermodynamic potentials (Groot and Mazur 1984): Temperature T [K] (or its inverse $1/T$ as the actual driving force); Pressure [Pa] divided by temperature (p/T) [Pa K^{-1}]; Chemical potential divided by temperature (μ/T) [J mol^{-1} K^{-1}]. At equilibrium between ice (i) and water (w) phases, with no gravity and no fluxes: $T_i = T_w$, $p_i = p_w$ and $\mu_i = \mu_w$

Two senses of "equilibrium" are used throughout the paper. The treatment is one of irreversible thermodynamics: the system as a whole is not at equilibrium, and gradients of $1/T$, p/T and μ/T drive the fluxes. However, every constitutive relation below assumes local equilibrium (Groot and Mazur 1984), i.e., each REV is internally at equilibrium at every instant, so that enthalpy, chemical potential and the SFCC relation $\theta_w(T)$ remain well defined at every point. The framework is thus non-equilibrium at the Darcy scale and equilibrium at the pore scale. That is the standard practice, but in a freezing soil it is a strong assumption. Section 3 gives the timescale condition it requires and where it fails.

The chemical potential, as we will see later, emerges as the unifying concept driving both phase transitions and water movement in partially frozen soil, encompassing effects of temperature, pressure, and composition.

The internal energy of a soil control volume is expressed as the sum of contributions from each constituent phase (Callen 1985; Lu and Godt 2012): $U = U_w + U_i + U_s + U_a$ where subscripts w, i, s, and a denote liquid water, ice, soil particles, and air respectively. Internal energy is an extensive property, meaning it scales linearly with system size and is therefore additive across phases. This additivity holds for any control volume over which the thermodynamic continuum approximation remains valid from the molecular scale upward. The lower limit is set by the requirement of sufficient molecular populations for statistical mechanics to apply, typically 10^6–10^9 molecules, corresponding to characteristic dimensions of 10^{-8}–10^{-7} m (Hill 1963). Above this threshold, thermodynamic laws apply at the pore scale. At larger scales (10^{-3}–10^{-1} m), the Darcy-scale approximation further permits the treatment of soil as an equivalent continuum (Bear 1972).

Under the hypothesis of negligible external pressure variations, it is convenient to work with enthalpy rather than internal energy. The two formulations are connected through a Legendre transformation (Callen 1985; Dall'amico 2010), which implies a change of independent variables from entropy (S), volume (V) and mole number (N) to temperature (T), pressure (p) and N. Enthalpy offers the practical advantage of being directly related to measurable quantities (temperature and heat capacity) without requiring explicit treatment of entropy.

The total enthalpy per unit volume is:

$$H = C_p(T - T_{ref}) + \sum_{\alpha} \rho_\alpha \theta_\alpha h_\alpha \tag{1}$$

where $C_p = \sum_\alpha \rho_\alpha \theta_\alpha c_{p,\alpha}$ is the bulk heat capacity at constant pressure, T is temperature, T_{ref} a reference temperature both in Kelvin, ρ_α the density, θ_α the volumetric fraction, $c_{p,\alpha}$ the specific heat

capacity, and h_α the reference specific enthalpy of phase $\alpha \in \{w, i, s, a\}$. The first term represents sensible heat storage, while the second captures the enthalpy associated with phase composition.

Since enthalpy is defined up to an arbitrary reference, we set the specific enthalpy of ice to zero. Equation 1 then simplifies to:

$$H = \sum_{\alpha \in \{w,i,a,s\}} \rho_\alpha \theta_\alpha c_{p,\alpha} (T - T_{ref}) + \rho_w \theta_w \ell_f \tag{2}$$

where ℓ_f [J kg^{-1}] is the specific latent heat of fusion. Two latent heats appear in this paper and are consistently distinguished: the specific latent heat $\ell_f \approx 3.34 \times 10^5$ J kg^{-1}, used wherever the balance is written per unit mass or per unit volume (Eqs. 2, 17, 28), and the molar latent heat $\mathcal{L}_f = M_w \ell_f \approx 6012$ J mol^{-1}, used wherever the balance is written per mole, i.e. in the chemical-potential relations (Eqs. 15–16 and 22–23). This expression can be inverted to obtain temperature as a function of enthalpy and water content. Such an inversion is advantageous because enthalpy, being a conserved quantity, is better suited as the primary state variable, while temperature T, liquid water content θ_w, and ice content θ_i are recovered from H and the total water content $\theta^{tot} = \theta_w + \theta_i$ (Tubini et al. 2021).

Upscaling the energy content of frozen soil is straightforward since all quantities involved are extensive. However, writing the dynamic equations requires upscaling energy and water fluxes to the Darcy scale, which demands further assumptions. In particular, the temperature at which the phase partition in Eq. 2 switches is not the arbitrary reference T_{ref}, a constant of convenience here taken as $T_{ref} = T_0 = 273.15$ K, but the local freezing temperature T^*, which in soils is not constant but depends on the size of the pores that are freezing and on the state of the water they contain. This dependence couples the energy and mass budgets and introduces the complexity discussed in the following sections.

The energy conservation equation, expressed in terms of enthalpy, takes the form:

$$\frac{\partial H}{\partial t} + \nabla \cdot \mathbf{J}_H = Q \tag{3}$$

where $\mathbf{J}_H$ represents the total energy flux and Q denotes volumetric source and sink terms. Once Eq. 3 is solved for enthalpy H, the temperature T can be recovered provided the local freezing temperature T^* is known from the Soil Freezing Characteristic Curve. This coupling between thermal evolution and phase kinetics constitutes the core complexity of freezing soil dynamics (Dall'Amico et al. 2011; Tubini et al. 2021).

The total energy flux comprises two contributions:

$$\mathbf{J}_H = \mathbf{J}_T + \rho_w h_w \mathbf{J}_w \tag{4}$$

where $\mathbf{J}_T$ is the conductive heat flux and the second term represents advective energy transport by water, with h_w being the specific enthalpy of water and $\mathbf{J}_w$ the water flux discussed in Sect. 3. The conductive flux follows Fourier's law:

$$\mathbf{J}_T = -\lambda_{eff} \nabla T \tag{5}$$

where λ_{eff} [W m^{-1} K^{-1}] is the effective thermal conductivity, which depends on the volumetric fractions and thermal conductivities of all phases present (water, ice, soil particles, and air). Various mixing models exist for estimating λ_{eff} from phase composition (Farouki 1981; Johansen 1975).

Equation 3 requires boundary conditions at the top and bottom of the soil domain. At the upper boundary, the energy balance includes radiative fluxes (shortwave and longwave), turbulent exchanges with the atmosphere (sensible heat flux and latent heat flux associated with evapotranspiration), and advective input from precipitation:

$$\mathbf{J}_H \cdot \mathbf{n}\big|_{z=0} = R_{net} - H_s - \lambda E + \rho_w h_w(T_p) P \tag{6}$$

where R_{net} is net radiation, H_s is sensible heat flux, λE is latent heat flux, T_p is precipitation temperature, $h_w(T_p)$ the specific enthalpy of water evaluated at that temperature, and P is precipitation rate. More complicated is the energy dynamic when it snowfalls (Endrizzi et al. 2014). At the lower boundary, either a prescribed geothermal heat flux or a fixed temperature condition may be imposed, depending on the depth of the domain and the timescale of interest.

3 Advection of Enthalpy in Freezing Conditions

Fluxes in unsaturated conditions are usually described by the Darcy-Buckingham law (Buckingham 1907; Richards 1931b). This relationship can be viewed either as an empirical finding or as a derivation from

fundamental principles under appropriate upscaling assumptions (Whitaker 1986). While forces acting at the thermodynamic scale can be derived as gradients of thermodynamic potentials, valid from approximately 10^{-8} m upward, an upscaling procedure is required to operate at the Darcy scale (10^{-3}–10^{-1} m), the macroscopic scale at which soil is treated as an equivalent continuum.

The potentials are generally written as heads [m] in hydrology and as pressures [Pa] in physical chemistry, and both are needed below, so four quantities are distinguished throughout: the matric potential as a pressure, ψ_p [Pa], negative in unsaturated soil; the suction $s = -\psi_p$ [Pa], which is positive; the pressure head $\psi = \psi_p/(\rho_w g)$ [m]; and the hydraulic head $(\psi + z)$ [m], the pressure head plus the elevation head z. The conversion between pressure and head is by the factor $\rho_w g \approx 9.81$ kPa m^{-1}. With this convention, the Darcy–Buckingham law (Eq. 7) and the relation to the chemical potential (Eq. 8) are written in heads, whereas the Young–Laplace equation (Eq. 10), the activity–pressure relation (Eq. 14), the retention models (Eqs. 25–26) and the generalised Clausius–Clapeyron mapping (Eq. 28) are written in pressures. Finally, ψ_p is the matric part alone. Osmotic effects enter the chemical potential separately, through the water activity (Eq. 11). The "total potential" of the soil-physics literature is therefore μ_w, with matric, osmotic and gravitational ($\rho_w g z$) components.

Assuming that ice and vapour fluxes are negligible, the water flux is expressed by the Darcy-Buckingham law as:

$$\mathbf{J}_w = -K(\theta_w, \theta_i)\nabla(\psi + z) \tag{7}$$

where $K(\theta_w, \theta_i)$ [m s^{-1}] is the hydraulic conductivity of the soil, which depends on both liquid water and ice contents, and $(\psi + z)$ [m] is the hydraulic head, comprising the pressure head ψ and the elevation head z. This simplification is appropriate when liquid water content is above the residual value and temperatures remain within a few degrees below 0°C, conditions typical of temperate permafrost and seasonal freeze-thaw cycles. For very cold or very dry frozen soils, vapour diffusion driven by ice-vapour pressure gradients can dominate mass transport, a regime outside the scope of this framework. For frost heave and ice-lens formation, the present framework provides the thermodynamic driving force (gradient of water chemical potential) but not the mechanical closure. That requires the premelting-dynamics framework of Rempel et al. (2004).

In the engineering literature (Michalowski and Zhu 2006; Stuurop et al. 2021), "cryosuction" is the migration of liquid water toward a freezing front and follows naturally from Eq. 7: the gradient in hydraulic head $\nabla(\psi + z)$ that drives flow is itself set by the gradient in chemical potential (Eq. 8), which in turn reflects the freezing-point depression field. No additional force is introduced. Cryosuction is the thermodynamic gradient of the water chemical potential expressed at the Darcy scale, fully consistent with the premelting-dynamics derivation of Rempel et al. (2004). The total hydraulic head is related to the total chemical potential of water by:

$$(\psi + z) = \frac{\mu_w}{\bar{v}_w \rho_w g} \tag{8}$$

where μ_w [J mol^{-1}] is the chemical potential of water, $\bar{v}_w$ [m^3 mol^{-1}] is the molar volume of water, ρ_w [kg m^{-3}] is water density, and g [m s^{-2}] is gravitational acceleration. The quotient $\mu_w/\bar{v}_w$ has units of pressure, and division by $\rho_w g$ converts it to a head, so that both sides of Eq. 8 are in metres, consistently with Eq. 7.

The pressure head ψ entering Eqs. 7 and 8 requires careful interpretation in light of the equilibrium assumptions stated above. At the Darcy scale, each representative elementary volume (REV) is treated as a point endowed with a statistical distribution of pore sizes. Within each REV, water is assumed to redistribute instantaneously among pores, filling them sequentially from largest to smallest until equilibrium is attained that is, until all filled pores share the same water potential, corresponding to that of the largest filled pore class. This internal equilibration is assumed to occur on a timescale much shorter than that governing inter-REV fluxes.

Fluxes between adjacent REVs are then driven by gradients in the pressure head of these larger filled pores. In other words, the macroscopic treatment decouples intra-REV dynamics (assumed instantaneous) from inter-REV transport (governed by Eq. 7). While this formulation is widely adopted and operationally effective, it embodies a strong assumption that pore-scale redistribution within

each control volume equilibrates infinitely fast relative to the advective transport between control volumes. Relaxing this assumption would require a non-equilibrium formulation capable of tracking the transient filling and draining of individual pore classes (Hassanizadeh and Gray 1993; DiCarlo 2013).

This single hypothesis carries the whole Darcy-scale construction, so it is worth stating quantitatively. Let τ_{intra} denote the time required for liquid water to redistribute among the pore classes within one REV, and τ_{inter} the time over which fluxes from neighbouring REVs change its water content appreciably. The formulation used here is valid only in the limit

$$\mathrm{Da}_c = \frac{\tau_{intra}}{\tau_{inter}} \ll 1, \tag{9}$$

that is, when equilibration inside an REV is fast compared with inter-REV transport. Da_c is a Damköhler-type ratio, comparing an internal rate with a transport rate. The same dimensionless group controls the Chapman–Enskog reduction of the kinetic theory of (Rigon 2026a), in which Richards' equation emerges as the leading order and the expansion fails when the group is not small. Neither timescale is a material constant. Because τ_{intra} scales inversely with the unsaturated conductivity of the films and throats connecting pore classes, it grows by orders of magnitude as the soil dries and as texture becomes finer, which is precisely the regime in which adsorbed films, rather than capillary menisci, control retention (Sect. 4). Dynamic-capillarity experiments imply relaxation times ranging from the order of minutes in wet coarse sands to the order of days in fine-textured materials (Hassanizadeh and Gray 1993; DiCarlo 2013), whereas τ_{inter} in a freezing soil column is set by the propagation of the thermal front and is itself typically of order hours to days. The two timescales are therefore not always well separated, and Eq. 9 should be regarded as a modelling hypothesis to be verified a posteriori for the soil and the forcing at hand, not as an established property of soils in general.

Freezing adds two requirements that have no counterpart in drying. First, the latent heat released as a pore class freezes must be conducted away fast enough for the REV to stay isothermal. Otherwise gradients develop inside the REV, which is what local equilibrium excludes. Second, nucleation must not be rate limiting, i.e., the supercooling needed to nucleate ice in the largest water-filled pore must be small compared with the freezing point depression of that pore. Both supercooling of a few tenths of a kelvin and hysteresis between the freezing and thawing branches of the SFCC are routinely observed (Watanabe and Flury 2008; Zhang et al. 2022; Kurylyk and Watanabe 2013), so the second requirement is not always met. In that case θ_w is no longer a single-valued function of T, and a rate equation for the phase change must replace the equilibrium SFCC. The framework developed here is thus the equilibrium limit of a more general rate-dependent theory, not that theory itself.

Under the equilibrium hypotheses stated above, pore filling follows an ordered sequence determined by the pore size distribution. For a given total water content in unfrozen conditions, water occupies pores sequentially from smallest to largest, as illustrated in the left panel of Fig. 1.

This framework, while enabling a tractable mathematical treatment of variably-saturated flow, constitutes a simplification. A new non-equilibrium theory has recently been proposed (Rigon 2026a, a), building on the conceptual foundations identified earlier (Hassanizadeh and Gray 1993; Gray and Miller 2015). It describes pore filling by a kinetic equation whose hydrodynamic limit returns the Richards equation. However, that theory is still under review and awaits confirmation, so the equilibrium treatment is retained here.

The largest pores correspond to the lowest absolute values of water potential (highest energy state) and therefore require the least energy withdrawal to freeze their content. Consequently, as energy is extracted from the soil, freezing proceeds from the largest pores inward, as shown in the right panel of Fig. 1: ice (red) progressively occupies larger pores while liquid water (blue) remains in smaller pores where it is held at lower potential. The thermodynamic basis for this sequential freezing is detailed in Sect. 4.

A direct consequence of ice formation is that liquid water content decreases, altering the relationship between θ_w and hydraulic head ψ. This raises the question of how to parameterise hydraulic properties in partially frozen soils. The simplest and most widely adopted approach is the "freezing equals drying" hypothesis (Koopmans and Miller 1966; Spaans and

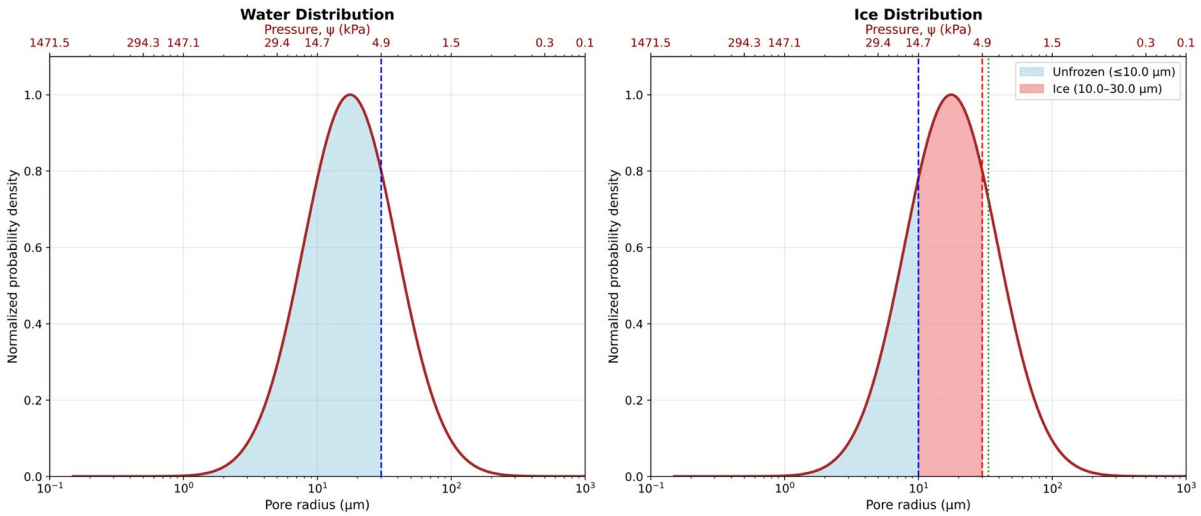


Fig. 1 Schematic of ordered pore filling and freezing in soil. Left panel: unfrozen conditions, where water (blue) fills pores from smallest to largest according to the soil water retention curve. Right panel: partially frozen conditions, where ice (red) occupies the largest pores while liquid water remains in the smallest pores. The pore size distribution is assumed log-normal following Kosugi's theory (Kosugi 1996)

Baker 1996; Dall'Amico et al. 2011), which exploits the analogy between ice-filled and air-filled pores: in both cases, the pore volume is occupied by a phase that does not participate in liquid water flow. Under this assumption, ice is treated as a passive obstruction equivalent to air, and the unfrozen soil water retention curve $\psi(\theta_w)$ remains valid when expressed in terms of liquid water content alone, regardless of ice content. Similarly, the hydraulic conductivity function $K(\theta_w)$ retains its unfrozen form. This approach requires no additional parameterisation and preserves the mathematical structure of the Richards equation, though it neglects effects such as pore blockage by ice and cryosuction-driven moisture redistribution (Watanabe and Flury 2008; Rempel 2007).

Because the analogy carries so much of the framework, its limits should be stated explicitly. "Freezing = drying" is exact only if: (i) ice is mechanically passive, so that the skeleton is neither deformed nor displaced as ice grows, which excludes frost heave and ice lensing (Rempel et al. 2004; Dash et al. 2006; ii) the ice–water interface takes the same geometry an air–water interface would take at the same liquid content, so that the two interfacial tensions differ only by a constant factor and the contact angle is unchanged; (iii) solutes are not excluded from the advancing ice, so that the osmotic contribution does not evolve as freezing proceeds; (iv) freezing and thawing follow the same path; and (v) the timescale condition of Eq. 9 holds. Each is violated to some degree. Solute exclusion concentrates the residual liquid and depresses T^* below the value predicted from the unfrozen SWRC, increasingly so as freezing advances and most strongly in saline soils. Ice in pore throats reduces connectivity more than the same volume of air, which is why empirical impedance factors are added to $K(\theta_w, \theta_i)$ in practice (Watanabe and Flury 2008; Kurylyk and Watanabe 2013; Stuurop et al. 2021). Hysteresis between freezing and thawing is observed systematically (Zhang et al. 2022, 2022b). The results below are therefore accurate where Eq. 9 holds, where the soil is not saline, and where the liquid content is high enough for the residual films to remain continuous, and progressively biased outside those conditions.

4 Phase Transitions and Freezing Point Depression

As anticipated above, freezing in porous media is not a discrete event occurring at a single temperature. Rather, the freezing point (T^*) varies across pore classes, following a sequential pattern determined by

the energetic states of water in different pore sizes. Water exists at different energy levels depending on pore geometry and surface interactions. The smallest pores, with the most negative matric potential (highest binding energy), retain liquid water to the lowest temperatures and are therefore the last to freeze. Quantitatively, the ordering follows from Eq. 28, which maps each value of the matric potential onto a distinct freezing temperature. The first water to freeze resides in the largest pores, where it is least bound to soil particles. Freezing then proceeds progressively into smaller pores, where stronger capillary and adsorptive forces depress the freezing point.

While this framework can be generalised to include all forces acting on water, we illustrate here first the case of capillary forces alone. Following Kosugi's theory (Kosugi 1996), the pore size distribution can be approximated as log-normal, as illustrated in Fig. 1, left panel. Under the equilibrium upscaling assumptions discussed in Sect. 3 (Millington and Quirk 1961; Mualem 1976), a given water content corresponds to the sequential filling of pores from smallest to largest, with only the highest-energy states (largest filled pores) governing water movement at the REV scale. For these pores, the Young-Laplace equation (Young 1805; Laplace 1805) establishes a relationship between pore radius (or meniscus curvature) and matric potential:

$$\psi_p = -\frac{2\sigma \cos\alpha}{r} \tag{10}$$

where σ is the surface tension of water, α is the contact angle, and r is the pore radius. The negative sign indicates that suction (negative pressure relative to atmospheric) increases as pore radius decreases. Consistently with the convention fixed in Sect. 3, the left-hand side of Eq. 10 is a pressure [Pa], not a head: the corresponding pressure head is $\psi = \psi_p/(\rho_w g)$ [m] and the suction is $s = -\psi_p = 2\sigma\cos\alpha/r > 0$ [Pa].

For a system containing water and possibly solutes, the chemical potential of water is Denbigh (1981):

$$\mu_w = \mu_w^0(T,P) + RT\ln(a_w) \tag{11}$$

where $\mu_w^0(T,P)$ is the chemical potential of pure water at temperature T and external pressure P, R is the universal gas constant, and a_w is the water activity, which accounts for osmotic, capillary, and adsorptive effects.

At equilibrium between ice and liquid water, the fundamental principle of phase equilibrium requires equality of chemical potentials (Gibbs n.d.):

$$\mu_w^0(T,P) + RT\ln(a_w) = \mu_{ice}^0(T,P) \tag{12}$$

where $\mu_w^0(T,P)$ and $\mu_{ice}^0(T,P)$ are the chemical potentials of pure water and ice at temperature T and pressure P, respectively.

The logarithmic dependence on activity in Eq. 12 is not merely empirical but emerges from fundamental statistical mechanics (Huang 1987; McQuarrie 2000).

This statistical mechanical foundation has important implications for freezing soil physics: the logarithmic form ensures that even trace amounts of solutes or confinement effects (which modify activity) produce finite depressions of the freezing point, and that the freezing point depression diverges logarithmically as water activity approaches zero in extremely dry or saline conditions.

The water activity can be decomposed into contributions from different mechanisms:

$$\begin{aligned}\ln(a_w) = {} & \ln(a_{w,osmotic}) + \ln(a_{w,capillary}) \\ & + \ln(a_{w,adsorption})\end{aligned} \tag{13}$$

This additivity follows from the product rule for activities: $a_w = a_{w,osmotic} \times a_{w,capillary} \times a_{w,adsorption}$, so $\ln(a_w) = \sum_i \ln(a_{w,i})$. The decomposition is exact when the three mechanisms act on physically distinct water populations (bulk dissolved, capillary-meniscus, and adsorbed-film water) and represents a first-order approximation in the general case. Cross-terms become significant in nanopores where all mechanisms overlap simultaneously.

For simplicity, we consider first the action of capillary forces alone. The pressure difference across a curved ice-water interface is governed by Eq. 10. The relationship between activity and pressure gives (Hill 1986):

$$\ln(a_{w,capillary}) = \frac{\bar{v}_w \psi_p}{RT} = -\frac{2\bar{v}_w \gamma_{iw}}{rRT} \tag{14}$$

where the negative sign reflects that suction ($\psi_p < 0$) reduces water activity ($\ln a_w < 0$), consistent with freezing-point depression. Here $\bar{v}_w$ is the molar volume of water and $\gamma_{iw} = \sigma\cos\alpha$ is the ice-water interfacial tension. Note that ψ_p, and not the pressure head ψ, enters Eq. 14: the product $\bar{v}_w\psi_p$ [J mol^{-1}] is

an energy per mole, so that the argument of the logarithm is dimensionless.

The difference in chemical potential between pure water and ice varies with temperature according to the Gibbs-Helmholtz relation (Callen 1985):

$$\frac{d(\mu_w^0 - \mu_{ice}^0)}{dT} = -\frac{\mathcal{L}_f}{T} \tag{15}$$

where $\mathcal{L}_f$ [J mol^{-1}] is the molar latent heat of fusion ($\mathcal{L}_f \approx 6012$ J mol^{-1}). For small temperature changes from the bulk freezing point T_0 to the depressed freezing point T^*, integration yields (Atkins et al. 2018):

$$\frac{\mathcal{L}_f(T^* - T_0)}{T_0} \approx RT^* \ln(a_w) \tag{16}$$

Considering only the capillary contribution and rearranging, we obtain the Gibbs-Thomson equation:

$$T^* - T_0 = -\frac{2T_0\gamma_{iw}}{\rho_i \ell_f r} \tag{17}$$

where T^* is the freezing temperature in a pore of radius r, $T_0 = 273.15$ K is the freezing temperature of bulk water, $\gamma_{iw} \approx 0.029$ J m^{-2} is the ice-water interfacial tension, $\rho_i \approx 917$ kg m^{-3} is ice density, and $\ell_f \approx 334\,000$ J kg^{-1} is the specific latent heat of fusion. Substituting these values, the freezing point depression is approximately:

$$\Delta T \approx -\frac{K_{GT}}{r}, \qquad K_{GT} = \frac{2T_0\gamma_{iw}}{\rho_i \ell_f} \approx 5.2 \times 10^{-8}\ \text{K m} = 0.052\ \text{K}\,\mu\text{m} \tag{18}$$

with r expressed in metres and K_{GT} in K m, or equivalently $\Delta T \approx -0.052/r$ with r in micrometres. The coefficient K_{GT} follows directly from the constants quoted above and is the value used in Fig. 2. The value of K_{GT} depends on the ice–water interfacial tension adopted and on the assumed interface geometry.

For a pore of radius $r = 1$ μm, this yields $\Delta T \approx -0.052$ K, a negligible depression. However, for nanometre-scale pores ($r = 10$ nm $= 0.01$ μm), the depression reaches $\Delta T \approx -5.2$ K. At these small pore sizes, however, adsorption forces begin to dominate over capillary effects, as discussed below.

When solutes are present, an additional contribution to freezing point depression arises. For ideal solutions, the osmotic contribution to water activity follows Raoult's law (Raoult 1886):

$$\ln(a_{w,osmotic}) = \ln(x_w) \approx -\frac{n_s}{n_w} \tag{19}$$

where x_w is the mole fraction of water, n_w is moles of water, and n_s is moles of solute. The osmotic pressure relates to solute concentration through the van 't Hoff equation (Hoff 1887):

$$\pi = i \cdot c \cdot R \cdot T \tag{20}$$

where i is the van 't Hoff factor, defined as the number of dissolved particles produced per formula unit upon dissociation (e.g. $i = 2$ for NaCl, which dissociates into Na^+ and Cl^-; $i = 1$ for non-electrolytes), and c [mol m^{-3}] is the molar concentration of solute.

Combining the osmotic and capillary contributions, the total freezing point depression becomes:

$$\Delta T_f = \Delta T_{f,osmotic} + \Delta T_{f,capillary} \tag{21}$$

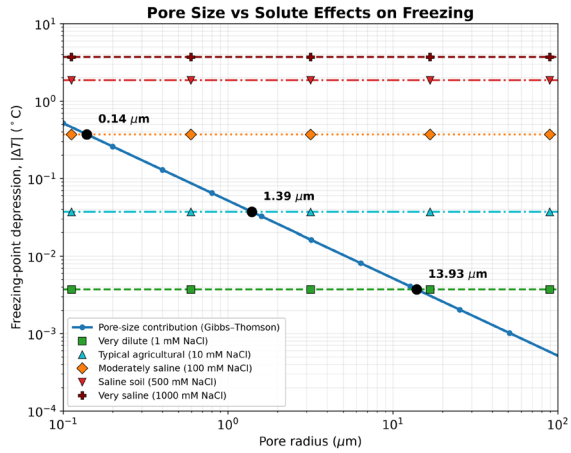


Fig. 2 Illustration of the physical (pore-size) and chemical (solute) contributions to freezing point depression (ΔT). The blue curve shows the Gibbs-Thomson effect ($K_{GT} = 0.052$ K μm, computed from Eq. 18), with smaller pore radii increasing $|\Delta T|$ hyperbolically as $1/r$. Horizontal dashed lines represent osmotic depression for various NaCl concentrations. Intersection points (black dots) define the equivalent pore radius for each salinity level. For example, a 0.14 μm pore exhibits the same freezing point depression as a 100 mM NaCl solution, a 1.39 μm pore that of a 10 mM solution, and a 13.9 μm pore that of a 1 mM solution. The 500 and 1000 mM levels intersect the curve below the plotted range of pore radii. NaCl is used as the illustrative solute with van 't Hoff factor $i = 2$, and the framework applies to any dilute ideal solution

The osmotic term is obtained by substituting Raoult's law $\ln a_{w,osmotic} \approx -i\,c\,\bar{v}_w$ into Eq. 16, and using $\ell_f = \mathcal{L}_f / M_w$, giving

$$\Delta T_{f,osmotic} = -\frac{iRT_0^2 \bar{v}_w c}{\mathcal{L}_f} = -\frac{iRT_0^2 c}{\rho_w \ell_f} \tag{22}$$

$$\Delta T_{f,capillary} = -\frac{2\gamma_{iw} T_0 \bar{v}_i}{r\mathcal{L}_f} = -\frac{2\gamma_{iw} T_0}{\rho_i \ell_f r} \tag{23}$$

The two forms in each of Eqs. 22 and 23 are equivalent, the first being written per mole and the second per unit mass. The molar volume entering Eq. 22 is that of water, $\bar{v}\mathrm{w} = \mathrm{Mw}/\rho_\mathrm{w}$, because the solute resides in the liquid, whereas Eq. 23 carries the molar volume of ice, $\bar{v}\mathrm{i} = \mathrm{Mw}/\rho_\mathrm{i}$, because the curvature pressure is borne by the ice. For NaCl at concentrations typical of agricultural soils (1–10 mM), $|\Delta T_{f,osmotic}| \approx 0.004$–$0.04$ K; for saline soils (100–1000 mM), $|\Delta T_{f,osmotic}| \approx 0.4$–$4$ K; for hypersaline permafrost (seawater-equivalent ~600 mM), $|\Delta T_{f,osmotic}| \approx 2.2$ K.

Figure 2 illustrates both contributions. The curve shows the Gibbs-Thomson effect as a function of the pore radius, while horizontal lines represent the osmotic depression for various NaCl concentrations. The intersection points define the equivalent pore radius for each salinity level: a pore of a given radius produces the same freezing point depression as a solution of the corresponding concentration. In saline soils the osmotic term is not a correction to the capillary one but the dominant contribution. Matching the depression of a 100 mM solution requires a pore of radius 0.14 μm, and matching a 500 mM solution requires one of about 0.03 μm.

However, experimental observations reveal that even the combined Gibbs-Thomson and osmotic effects cannot fully explain measured freezing point depressions, particularly in fine-textured soils where liquid water persists at temperatures far below those predicted by Eq. 21 (Devoie et al. 2022). This discrepancy points to a fundamental limitation of capillary-based theories.

According to recent work by Lu and colleagues (Lu 2016; Luo et al. 2022), the Young-Laplace equation adequately describes soil water retention only over a restricted range of suction, approximately $s < 0.1$ MPa. At higher suctions adsorptive forces dominate. Between about 0.1 and 10 MPa adsorbed films control water retention, and beyond 10 MPa tightly adsorbed water layers become significant. This limitation arises because at low water contents, water distributes in thin films over particle surfaces, where adsorption rather than capillarity governs retention.

Lu's framework (Lu 2016) recognises that pore-water pressure in soil arises from three physically distinguishable sources: ambient pressure, surface tension-induced capillary pressure, and electromagnetic potential-induced adsorptive pressure. The total water content is accordingly partitioned:

$$\theta(s) = \theta_a(s) + \theta_c(s) \tag{24}$$

where θ_a represents adsorbed water and θ_c represents capillary water, and where, following the convention of Sect. 3, the retention models are written in terms of the positive suction $s = -\psi_p$ [Pa], as in the original formulation of Lu (2016). The adsorptive component can be modelled as Lu (2016):

$$\theta_a(s) = \theta_{a,max}\left\{1 - \left[\exp\left(-\frac{s_{max} - s}{s}\right)\right]^m\right\} \tag{25}$$

where $\theta_{a,max}$ is the maximum adsorbed water content, s_{max} is the maximum (oven-dry) suction, and m governs the rate of change in adsorption. Equation 25 is the adsorption model of Lu (2016) written in terms of the positive suction s, with the exponent m applied to the exponential. For any $m > 0$ it gives $\theta_a = \theta_{a,max}$ at zero suction and $\theta_a = 0$ at $s = s_{max}$. The capillary component follows:

$$\theta_c(s) = \frac{1}{2}\left[1 - \mathrm{erf}\left(\sqrt{2}\cdot\frac{s - s_c}{s_c}\right)\right] \cdot \left[\theta_{sat} - \theta_a(s)\right] \cdot \left[1 + (\alpha_{vG} s)^n\right]^{\frac{1}{n}-1} \tag{26}$$

where θ_{sat} is the saturated water content, s_c [Pa] is the mean cavitation suction and α_{vG} [Pa^{-1}], n [–] are pore size distribution parameters. The subscript distinguishes this parameter from the contact angle α of Eq. 10.

The preceding derivations establish how the freezing point T^* depends on pore radius, solute concentration, and film thickness through the three contributions to freezing point depression.

To complete the connection with the enthalpy formulation, we require the Soil Freezing Characteristic Curve (SFCC), which describes the

equilibrium liquid water content θ_w as a function of temperature T for $T < T_0$.

At any temperature $T < T_0$: all pores (or film thicknesses) with freezing point $T^* > T$ contain ice; those with $T^* < T$ remain liquid-filled.

The liquid water content at temperature T is then the cumulative water content in all pores and films that remain unfrozen:

$$\theta_w(T) = \left(\theta^{tot} - \theta_{a,max}\right) \int_0^{r^*(T)} f(r)\, dr + \theta_a(T) \qquad (27)$$

where $f(r)$ [m^{-1}] is the pore-size probability density function (pdf) of the log-normal Kosugi distribution (Kosugi 1996), normalised so that $\int_0^\infty f(r)\, dr = 1$. The first term gives the capillary water held in pores with radius r < r*(T), those still liquid-filled at temperature T, the prefactor $\theta^{tot} - \theta_{a,max}$ being the capillary part of the total water content. Counting it this way keeps the two populations disjoint, as required by Eq. 24. The second term $\theta_a(T)$ is the adsorbed-water content from Eq. 25, evaluated at the suction s corresponding to T via Eq. 28. The critical radius $r^*(T)$ is that of the pore whose Gibbs–Thomson freezing point equals T, i.e. $r^*(T) = K_{GT}/(T_0 - T)$ from Eq. 18. Equation 27 is exact only to the extent that the capillary and adsorptive water populations are distinct, the same condition under which the activity decomposition of Eq. 13 is exact.

The SFCC can be derived from the Soil Water Retention Curve (SWRC) via the generalised Clausius-Clapeyron equation, which provides the thermodynamic link between total suction and freezing temperature. For water at suction s that freezes at temperature T^*, the relationship is Dall'Amico et al. (2011):

$$\psi_p(T^*) = \frac{\rho_w \ell_f}{T_0}(T^* - T_0) \qquad (28)$$

Both sides of Eq. 28 are pressures [Pa]. The equivalent statements in terms of the suction and of the pressure head are $s(T^*) = \rho_w \ell_f (T_0 - T^*)/T_0 > 0$ and $\psi(T^*) = \ell_f (T^* - T_0)/(g\, T_0)$ [m]. Numerically, $\rho_w \ell_f / T_0 \approx 1.22$ MPa K^{-1}, that is about 125 m of pressure head per kelvin of freezing point depression, which is why even a fraction of a degree of cooling corresponds to a suction far beyond the capillary range of the Young–Laplace equation and thus into the regime where the adsorptive terms of Eqs. 24–26 dominate.

Equation 28 establishes a one-to-one mapping between matric potential ψ_p and freezing-point depression $\Delta T = T^* - T_0$. Under the local-equilibrium assumption, a pore of radius r that is filled with water at matric potential $\psi_p = -2\gamma \cos\alpha / r$ will freeze precisely at the temperature $T^*(r)$ given by Eq. 17. The same water content that corresponds to a given ψ_p in the unfrozen SWRC therefore corresponds to the same water content in the frozen SFCC at the equivalent T^*. This isomorphism forms the basis of the "freezing = drying" hypothesis (Koopmans and Miller 1966; Dall'Amico et al. 2011) and has been confirmed mathematically by rigorous homogenisation (Peszynska et al. 2024a). Its key assumptions are: (i) rigid, non-deforming soil skeleton; (ii) no hysteresis between freezing and thawing paths; (iii) local thermodynamic equilibrium within each REV; (iv) no supercooling, i.e. nucleation is not rate-limiting; and (v) no solute exclusion at the ice front, so that the osmotic contribution does not change as freezing proceeds. Assumptions (i)–(v) are exactly those examined in Sect. 3. They are recalled here because they are inherited in full by every SFCC obtained through Eq. 29.

This relation allows the SFCC to be derived from a known SWRC by direct substitution:

$$\theta_w(T) = \theta_w\left(\psi_p(T)\right) = \theta_w\left(\frac{\rho_w \ell_f}{T_0}(T - T_0)\right) \qquad (29)$$

When Lu's adsorption-aware SWRC is used, the resulting SFCC automatically accounts for both capillary and adsorptive contributions to unfrozen water. The inclusion of the adsorptive potential explains the extreme freezing point depressions (down to −80°C) observed in clay nanopores.

Overall, it is essential to recognise that the SFCC $\theta_w(T)$ is a continuous, monotonically increasing function of temperature, not a step function at a single freezing point. As temperature decreases below T_0, progressively more water freezes as smaller pores and thinner adsorbed films reach their respective freezing points. It should be stressed that this monotonicity is a consequence of the equilibrium construction, not an observation. Because Eq. 29 maps a single-valued SWRC onto a single-valued SFCC, the resulting curve cannot represent the hysteresis and the

supercooling that measurements systematically show (Watanabe and Flury 2008; Zhang et al. 2022; Kurylyk and Watanabe 2013). Reproducing those features requires relaxing assumptions (ii) and (iv) above, which takes the problem outside the equilibrium framework developed here.

5 Conclusions

The enthalpy form of the energy budget, the Gibbs–Thomson and van 't Hoff relations, the adsorption-aware retention model of Lu and co-workers, and the generalised Clausius–Clapeyron mapping are all established results. This paper combines them into one internally consistent chain, expressed in a single notation, and states the conditions the combination requires. The four contributions are (i) a unified chemical-potential derivation of freezing point depression incorporating capillary, osmotic and adsorptive contributions; (ii) an explicit thermodynamic isomorphism between the SWRC and the SFCC via the generalised Clausius-Clapeyron equation, using Lu's adsorption-aware retention model; (iii) the connection of the resulting SFCC to the Darcy-scale enthalpy balance as a constitutive closure; and (iv) a timescale criterion, Eq. 9, that turns the local-equilibrium and instantaneous-redistribution hypotheses into a condition that can be tested. The framework is restricted to the pore-water subsystem within a rigid soil skeleton, and all derivations assume local thermodynamic equilibrium within each REV.

Freezing in porous media is sequential, and this is its central organising principle. It proceeds from the largest pores to the smallest, with the freezing point depression governed by capillary effects, solute concentration, nucleation barriers and surface adsorption together. The classical Gibbs-Thomson effect alone is insufficient for fine-textured soils, where liquid water persists far below capillary predictions, and the adsorption-aware framework of Lu and colleagues (Lu 2016; Luo et al. 2022) can account for the extreme depressions observed in clay nanopores.

The local equilibrium hypothesis underlying both the Darcy-Buckingham law and the freezing = drying analogy makes the problem tractable but is a strong simplification. It requires intra-REV redistribution to equilibrate much faster than inter-REV transport, stated here as $\mathrm{Da}_c = \tau_{intra}/\tau_{inter} \ll 1$ (Eq. 9) and expected to fail in fine-textured and dry soils (Hassanizadeh and Gray 1993; DiCarlo 2013). A non-equilibrium theory able to track dynamic pore filling has recently been proposed (Rigon 2026a, a) but is not yet established. Meanwhile freezing = drying is an effective parameterisation, though it neglects ice-induced pore blockage and cryosuction-driven redistribution. Cryosuction needs no force beyond the chemical-potential gradient already present in the Darcy-Buckingham equation, as shown in Sect. 3, and the premelting-dynamics framework of Rempel et al. (2004) gives the pore-scale derivation consistent with this view.

The enthalpy formulation has practical advantages. With enthalpy as the primary state variable, temperature locks naturally during the phase transition as energy fluxes are consumed by latent heat, and temperature is recovered through the SFCC, which encodes the pore size distribution and the associated freezing point depressions. The coupling this creates is the main source of complexity in freezing soil dynamics. The freezing point is set by suction and hence by water content, which is set by ice content, which depends in turn on temperature. For cold regions hydrology the consequences are direct, since ice formation reduces hydraulic conductivity and alters moisture redistribution, while latent heat exchange buffers temperature and controls how fast freeze-thaw fronts advance.

Three limitations define the work that remains. First, the paper is theoretical. The internal consistency of the chain from the SWRC through the SFCC to the enthalpy closure is established here, but its quantitative adequacy is untested. A companion paper will couple the closure to the Richards equation and test it against measured SFCC data, including datasets of the type reported by Devoie et al. (2022). Second, the equilibrium SFCC is single-valued by construction and cannot represent freezing–thawing hysteresis or supercooling, both routinely observed. The SFCC must then give way to a rate equation for the phase change, and identifying that rate law is, in our view, the central open problem in the field. Third, the mechanical problem is excluded by assumption, since frost heave and ice-lens formation require a momentum balance for the ice phase that the present treatment does not supply (Rempel et al. 2004; Dash et al. 2006).

Within these limits, the framework provides a self-consistent starting point whose assumptions can be tested.

Acknowledgements JMW and RR would like to thank and acknowledge funding from the "SPACE IT UP" project, ASI contract no. 2024-5-E.0, CUP master no. I53D24000060005, SAP fund no. 000040104905.

Author contributions All the Authors equally likely contribute to any part of the manuscript.

Funding Open access funding provided by Universit ├á degli Studi di Trento within the CRUI-CARE Agreement.

Data availability No datasets were generated or analysed during the current study.

Declarations

Conflict of interest The authors declare that they have no conflict of interest.

Open Access This article is licensed under a Creative Commons Attribution 4.0 International License, which permits use, sharing, adaptation, distribution and reproduction in any medium or format, as long as you give appropriate credit to the original author(s) and the source, provide a link to the Creative Commons licence, and indicate if changes were made. The images or other third party material in this article are included in the article's Creative Commons licence, unless indicated otherwise in a credit line to the material. If material is not included in the article's Creative Commons licence and your intended use is not permitted by statutory regulation or exceeds the permitted use, you will need to obtain permission directly from the copyright holder. To view a copy of this licence, visit http://creativecommons.org/licenses/by/4.0/.

References

Amankwah SK, Ireson AM, Maulé C, Brannen R, Mathias SA (2021) A model for the soil freezing characteristic curve that represents the dominant role of salt exclusion. Water Resources Research **57**(8) https://doi.org/10.1029/2021WR030070

Atkins PW, Paula J, Keeler J (2018) Atkins' Physical Chemistry, 11th edn. Oxford University Press, Oxford

Bear J (1972) Dynamics of Fluids in Porous Media. American Elsevier, New York

Buckingham E (1907) Studies on the movement of soil moisture. Technical Report Bulletin 38, USDA Bureau of Soils, Washington D.C

Callen HB (1985) Thermodynamics and an introduction to thermostatistics, 2nd edn. John Wiley & Sons, New York

Dall'Amico M, Endrizzi S, Gruber S, Rigon R (2011) A robust and energy-conserving model of freezing variably-saturated soil. Cryosphere 5:469–484. https://doi.org/10.5194/tc-5-469-2011

Dall'Amico M (2010) Coupled water and heat transfer in permafrost modeling. PhD thesis, University of Trento

Dash JG, Rempel AW, Wettlaufer JS (2006) The physics of premelted ice and its geophysical consequences. Rev Mod Phys 78:695–741. https://doi.org/10.1103/RevModPhys.78.695

Denbigh KG (1981) The Principles of Chemical Equilibrium, 4th edn. Cambridge University Press, Cambridge

Devoie AG, Gruber S, McKenzie JM (2022) A repository of measured soil freezing characteristic curves: 1921 to 2021. Earth System Science Data 14(7):3365–3377. https://doi.org/10.5194/essd-14-3365-2022

DiCarlo DA (2013) Stability of gravity-driven multiphase flow in porous media: 40 years of advancements: stability of multiphase gravity-driven flow. Water Resour Res 49(8):4531–4544. https://doi.org/10.1002/wrcr.20359

Dobinski W (2012) Permafrost: the contemporary meaning of the term and its consequences. Bull Geogr Phys Geogr Ser 5:29–42. https://doi.org/10.2478/v10250-012-0002-9

Endrizzi S, Gruber S, Dall'Amico M, Rigon R (2014) GEOtop 2.0:simulating the combined energy and water balance at and below the land surface accounting for soil freezing, snow cover and terrain effects. Geosci Model Dev 7(6):2831–2857. https://doi.org/10.5194/gmd-7-2831-2014

Farouki OT (1981) Thermal properties of soils. CRREL Monograph 81-1, U.S. Army Cold Regions Research and Engineering Laboratory, Hanover, NH

Gibbs JW On the equilibrium of heterogeneous substances. Transactions of the Connecticut Academy of Arts and Sciences 3, 108–248343524 (1876–1878)

Gray WG, Miller CT (2015) Introduction to the thermodynamically constrained averaging theory for porous medium systems. Springer, Cham

Groot SR, Mazur P (1984) Non-equilibrium thermodynamics. Dover Publications, New York

Hassanizadeh SM, Gray WG (1993) Thermodynamic basis of capillary pressure in porous media. Water Resour Res 29(10):3389–3405. https://doi.org/10.1029/93WR01495

Hill TL (1963) Thermodynamics of Small Systems. W. A, Benjamin, New York

Hill TL (1986) An Introduction to Statistical Thermodynamics. Dover Publications, New York

Hjort J, Karjalainen O, Aalto J, Westermann S, Romanovsky VE, Nelson FE, Etzelmüller B, Luoto M (2018) Degrading permafrost puts arctic infrastructure at risk by mid-century. Nat Commun 9(1):5147. https://doi.org/10.1038/s41467-018-07557-4

Hoff JH (1887) Die rolle des osmotischen druckes in der analogie zwischen lösungen und gasen. Z Phys Chem 1:481–508. https://doi.org/10.1515/zpch-1887-0151

Huang K (1987) Statistical Mechanics, 2nd edn. John Wiley & Sons, New York

Johansen O (1975) Thermal conductivity of soils. Norway,(PhD thesis)

Koopmans RWR, Miller RD (1966) Soil freezing and soil water characteristic curves. Soil Sci Soc Am J 30(6):680–685.

https://doi.org/10.2136/sssaj1966.03615995003000060011x
Kosugi K (1996) Lognormal distribution model for unsaturated soil hydraulic properties. Water Resour Res 32(9):2697–2703. https://doi.org/10.1029/96WR01776
Kurylyk BL, Watanabe K (2013) The mathematical representation of freezing and thawing processes in variably-saturated, non-deformable soils. Adv Water Resour 60:160–177. https://doi.org/10.1016/j.advwatres.2013.07.016
Laplace PS (1805) Traité de Mécanique Céleste. Supplément Au Dixième livre, Courcier, Paris
Lewkowicz AG, O'Neill HB, Wolfe SA, Roy-Léveillée P, Roujanski VE, Hoeve E, Gruber S, Brooks H, Rudy ACA, Koenig CEM, Brown N, Bonnaventure PP (2025) Glossary of permafrost science and engineering. Canadian Permafrost Association Ottawa ON. https://doi.org/10.3138/cpa-gpse
Lu N (2016) Generalized soil water retention equation for adsorption and capillarity. J Geotech Geoenviron Eng 142(10):04016051. https://doi.org/10.1061/(ASCE)GT.1943-5606.0001524
Lu N, Godt JW (2012) Hillslope Hydrology and Stability. Cambridge University Press, Cambridge
Lunardini VJ (1985) Freezing soil phase change occurring over finite temperature difference. Proceedings of the 4th International Offshore Mechanics and Arctic Engineering Symposium. ASME,
Luo S, Lu N, Zhang C, Likos W (2022) Soil water potential: a historical perspective and recent breakthroughs. Vadose Zone Journal 21(4):20203. https://doi.org/10.1002/vzj2.20203
McQuarrie DA (2000) Statistical Mechanics. University Science Books, Sausalito, CA
Michalowski RL, Zhu M (2006) Frost heave modelling using porosity rate function. Int J Numer Anal Meth Geomech 30(8):703–722. https://doi.org/10.1002/nag.497
Millington RJ, Quirk JP (1961) Permeability of porous solids. Trans Faraday Soc 57:1200–1207. https://doi.org/10.1039/TF9615701200
Mualem Y (1976) A new model for predicting the hydraulic conductivity of unsaturated porous media. Water Resour Res 12(3):513–522. https://doi.org/10.1029/WR012i003p00513
Muskat M, Meres MW (1936) The flow of heterogeneous fluids through porous media. Physics 7:346–363. https://doi.org/10.1063/1.1745403
Obu J, Westermann S, Bartsch A, Berdnikov N, Christiansen HH, Dashtseren A, Delaloye R, Elberling B, Etzelmüller B, Kholodov A, Khomutov A, Kääb A, Leibman MO, Lewkowicz AG, Panda SK, Romanovsky V, Way RG, Westergaard-Nielsen A, Wu T, Yamkhin J, Zou D (2019) Northern hemisphere permafrost map based on TTOP modelling for 2000–2016 at 1 km2 scale. Earth Sci Rev 193:299–316. https://doi.org/10.1016/j.earscirev.2019.04.023
Peszynska M, Hilliard Z, Vohra N (2024) Coupled flow and energy models with phase change in permafrost from pore- to darcy scale: modeling and approximation. J Comput Appl Math 450:115964. https://doi.org/10.1016/j.cam.2024.115964
Peszynska M, Vohra N, Bigler L (2024) Upscaling an extended heterogeneous stefan problem from the pore-scale to the darcy scale in permafrost. Multiscale Model Simul 22(1):436–475. https://doi.org/10.1137/23M1552000
Raoult FM (1886) Loi générale des tensions de vapeur des dissolvants. Comptes Rendus 104:1430–1433
Rempel AW (2007) Formation of ice lenses and frost heave. J Geophys Res Earth Surf 112(F2):02–21. https://doi.org/10.1029/2006JF000525
Rempel AW, Wettlaufer JS, Worster MG (2004) Premelting dynamics in a continuum model of frost heave. J Fluid Mech 498:227–244. https://doi.org/10.1017/S0022112003006761
Richards LA (1931) Capillary conduction of liquids through porous mediums. Physics 1(5):318–333. https://doi.org/10.1063/1.1745010
Rigon R (2026a) Richards' Equation as a Hydrodynamic Limit: Chapman–Enskog Reduction of the Continuum Kinetic Equation for Unsaturated Soil Water. arXiv preprint arXiv:2607.17358. https://doi.org/10.48550/arXiv.2607.17358
Rigon R (2026b) The Statistical Physics of Unsaturated Soil Water: Kinetic Theory and Non-Commutative Pore Water Dynamics. arXiv preprint arXiv:2607.09416. https://doi.org/10.48550/arXiv.2607.09416
Romanovsky VE, Osterkamp TE (2000) Effects of unfrozen water on heat and mass transport processes in the active layer and permafrost. Permafrost Periglac Process 11(3):219–239. https://doi.org/10.1002/1099-1530
Schuur EAG, McGuire AD (2015) Climate change and the permafrost carbon feedback. Nature 520:171–179. https://doi.org/10.1038/nature14338
Spaans EJA, Baker JM (1996) The soil freezing characteristic: its measurement and similarity to the soil moisture characteristic. Soil Sci Soc Am J 60(1):13–19. https://doi.org/10.2136/sssaj1996.03615995006000010005x
Stuurop JC, Zee SEATM, Voss CI, French HK (2021) Simulating water and heat transport with freezing and cryosuction in unsaturated soil: comparing an empirical, semi-empirical and physically-based approach. Adv Water Resour 149:103846. https://doi.org/10.1016/j.advwatres.2021.103846
Tubini N, Gruber S, Rigon R (2021) A method for solving heat transfer with phase change in ice or soil that allows for large time steps while guaranteeing energy conservation. Cryosphere 15:2541–2568. https://doi.org/10.5194/tc-15-2541-2021
Tubini N, Rigon R (2022) Implementing the water, HEat and transport model in GEOframe: algorithms, informatics(WHETGEO-1D v.1.0), design patterns, open science features, and 1D deployment. Geosci Model Dev 15(1):75–104. https://doi.org/10.5194/gmd-15-75-2022
Walvoord MA, Kurylyk BL (2016) Hydrologic impacts of thawing permafrost–a review. Vadose Zone Journal 15(6):2016–010010. https://doi.org/10.2136/vzj2016.01.0010
Wang C, Li K, Cai H, Wu Y, Lin Z, Li S (2023) Study of supercooling phenomena in soil-water systems based on nucleation theory: Quantifying supercooling degree.

Water Resources Research **59**(11) https://doi.org/10.1029/2023WR035935

Watanabe K, Flury M (2008) Capillary bundle model of hydraulic conductivity for frozen soil. Water Resour Res 44(12):12402. https://doi.org/10.1029/2008WR007012

Watanabe K, Osada Y (2016) Comparison of hydraulic conductivity in frozen saturated and unfrozen unsaturated soils. Vadose Zone J 15(5):1–7. https://doi.org/10.2136/vzj2015.11.0154

Wettlaufer JS, Worster MG (2006) Premelting dynamics. Annu Rev Fluid Mech 38:427–452. https://doi.org/10.1146/annurev.fluid.37.061903.175758

Whitaker S (1986) Flow in porous media I: a theoretical derivation of Darcy's law. Transp Porous Media 1(1):3–25. https://doi.org/10.1007/BF01036523

Young T (1805) An essay on the cohesion of fluids. Philos Trans R Soc Lond 95:65–87. https://doi.org/10.1098/RSTL.1805.0005

Zhang T, Barry RG, Knowles K, Heginbottom JA, Brown J (1999) Statistics and characteristics of permafrost and ground-ice distribution in the Northern Hemisphere. Polar Geogr 23(2):132–154. https://doi.org/10.1080/10889379909377670

Zhang C, Gou L, Hu S, Lu N (2022) A thermodynamic formulation of water potential in soil. Water Resour Res 58(9):2022–032369. https://doi.org/10.1029/2022WR032369

Zhang L, Yang C, Wang D, Zhang P, Zhang Y (2022) Freezing point depression of soil water depending on its non-uniform nature in pore water pressure. Geoderma 412(115724):115724. https://doi.org/10.1016/j.geoderma.2022.115724

Publisher's Note Springer Nature remains neutral with regard to jurisdictional claims in published maps and institutional affiliations.